Instabilities of molecule motion in a linear ac trap

Peter Lützow, Melanie Schnell,* and Gerard Meijer
Fritz-Haber-Institut der Max-Planck-Gesellschaft, Faradayweg 4-6, D-14195 Berlin, Germany
(Received 7 March 2008; published 3 June 2008)

The stability of a linear ac trap for neutral polar molecules is investigated both theoretically and experimentally. While the overall stability is found to be well described by the linearized equations of motion within the usual framework of stability diagrams, instabilities similar to those observed in anharmonic radio-frequency ion traps occur inside the nominal stable regions. These motional resonances are caused by strong anharmonic contributions to the trapping fields, that inevitably appear in ac traps for polar molecules. Nonlinear resonant energy transfer from the high-frequency source to molecules inside the trap is observed for the particles' fundamental frequency of transverse oscillation being $\frac{1}{4}$ of the forcing frequency.

DOI: 10.1103/PhysRevA.77.063402 PACS number(s): 37.10.Pq, 37.10.Mn, 33.15.−e

I. INTRODUCTION

Research on cold molecules is undergoing a rapid expansion, driven by the development of a variety of methods to create cold molecules [1]. The Stark deceleration method employs inhomogeneous electric fields to decelerate and trap neutral polar molecules [2] by exploiting the Stark effect, i.e., the interaction of the molecular dipole moment with an electric field. It has to be differentiated between molecules in states with a positive Stark effect, the so-called low-field seekers (LFSs), and molecules in states with a negative Stark effect, the high-field seekers (HFSs). Interestingly, all states of larger and heavier molecules are practically HFSs as well as the internal ground state of any molecule. Consequently, there is a large interest in decelerating and trapping molecules in high-field seeking states [3]. Especially experiments with trapped ground-state molecules are potentially fruitful because of the long interaction times that are possible even in very dense samples since decay through inelastic collisions is impossible. So far trapping of HFS molecules in optical dipole traps [4] as well as in ac traps of different geometries [5–7] has been experimentally demonstrated. In an optical dipole trap the focus of a high power laser attracts molecules in HFS states since, time-averaged, it constitutes a field maximum. However, optical dipole traps are shallow and the trapping volume is small. In addition, special care has to be taken to tune the trapping laser far away from a molecular resonance since heating through spontaneous emission is the important loss channel.

ac traps for polar molecules are the analogs to radio frequency traps for ions. By rapidly switching between different electrostatic fields that exhibit complementary saddlepoints in the trap center it is possible to dynamically stabilize the motion of HFS polar molecules. At a given time, molecules in such an arrangement are focused along certain directions while they are defocused along others. If in a subsequent configuration the directions of focusing and defocusing are interchanged, confinement of the particles can be achieved for well chosen switching frequencies and trap voltages. In this paper, we will investigate the stability of the molecules' motion in a linear ac trap [7] loaded from a Stark decelerator [8]. We will adopt the general principles of Floquet stability in the approximation of linear equations of motion, well known in particle accelerator or ion trap physics, for ac trapping of polar molecules. In addition, certain resonance features that arise through the presence of strong nonlinear forces, which cannot be avoided in ac traps, are discussed. These nonlinear motional resonances occur if the fundamental frequency of a particle's motion is a certain rational multiple of the forcing frequency. The purpose of the present investigation is to study resonance effects in order to identify the stable trapping regimes which are needed for future applications such as sympathetic and evaporative cooling, which are necessary steps to enter the ultracold regime ($T < 1$ mK) for molecules. Both methods are predicted to work only for ground state molecules so that ac traps are key tools. Furthermore, as was shown recently and which is an essential ingredient for sympathetic cooling, atoms can be trapped in ac electric traps as well [9]. In addition, a detailed understanding of resonance effects is necessary for a better understanding of ac trapping in general. And since the confinement principle in ac traps is similar to the ones in AG deceleration, which is the only method to decelerate also large molecules [3,10,11], and ac guiding [12,13], the results of our study are also valid for these techniques.

The structure of this article is as follows. In Sec. II the trapping principle is briefly discussed. In Sec. III we introduce the concept of stability and resonances for ac trapping of neutral polar molecules to set the stage for the analysis of the experimental results. The harmonic stability diagram of the linear ac trap including nonlinear resonances is determined. In Sec. IV the experimental setup and the experimental procedure are described. In Sec. V the theoretical and experimental results are jointly discussed and Sec. VI finally summarizes and concludes our investigation.

II. TRAPPING PRINCIPLE

The linear ac trap consists of four 8 mm long double rods with 3 mm diameter each in a quadrupole arrangement [Fig. 1(a)]. The electrodes of the trap are held using bent tantalum wires, that are suspended from a ceramic plate. This technique of holding allows one to place the trap's electrodes

*Corresponding author. schnell@fhi-berlin.mpg.de

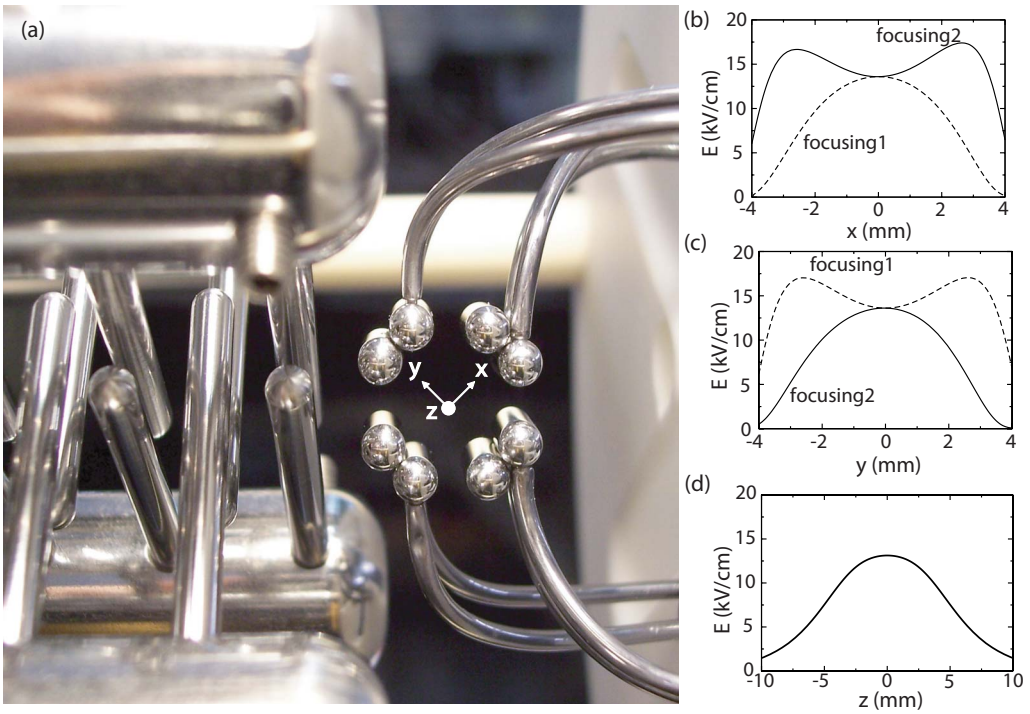

FIG. 1. (Color online) The trap and the electric field for the two focusing configurations in the x, y, and z directions. (a) Picture of the linear ac trap which is placed very close to the end of the decelerator, located in the left half of the picture. The corresponding coordinate system used for the theoretical description is also shown. (b) The electric field in the x direction and (c) in the y direction for focusing 1 and focusing 2, respectively. (d) The electric field in the z direction is the same for the two configurations (see text).

directly behind the Stark decelerator's electrodes making the trap an effective extension of the decelerator by one additional pair of electrodes. Molecules leaving the decelerator are already inside the trap without any free flight passage that would lead to loss of molecules. This leads to an improved loading of the molecules into the trap, as has been demonstrated and discussed in detail in Ref. [7].

By applying high voltages (up to ± 10 kV) to opposing electrodes on the y axis, while the other two on the x axis remain grounded, a saddle point of the electric field with a maximum along x and z directions and a minimum along the y direction [focusing 1, Figs. 1(b) and 1(c)] is generated in the center of the trap. Thus, molecules in HFS states are focused along x and z and are defocused along the y direction. By energizing the opposing electrodes on the x axis, with the other two switched to ground (focusing 2), the resulting field configuration is rotated by 90° about the z axis [Figs. 1(b) and 1(c)] compared to focusing 1. Consequently, molecules in HFS states are now focused along y and z while simultaneously being defocused along x. By switching between these two saddle point configurations HFS molecules experience alternating focusing and defocusing forces along the transverse directions while the force along z, which is not affected by the switching, remains focusing throughout the whole switching sequence. To a first approximation the motion along z is therefore solely determined by a static harmonic potential well and may thus be disregarded when discussing the dynamical stability of molecular trajectories due to the high frequency switching. However, the fact that the electric field has a maximum along z influences the transverse motion indirectly since the divergence of the force on a HFS molecule must vanish in a saddlepoint [14]. The advantage of a static focusing force along z therefore comes hand in hand with a necessary decrease of the focusing strength in the transverse directions. Therefore, the linear force constant characterizing the transverse focusing will always be smaller or equal to the force constant of transverse defocusing.

Nevertheless, stable trapping is possible since the magnitude of the force on a molecule increases with its distance from the center as long as the amplitude of the trajectory does not exceed a maximum value. Molecules that move toward the center of the trap under the influence of a focusing force will be closer to the center, where the force is smaller, when the defocusing force is applied. This defocusing force will move the molecules further away from the center again, bringing them in a region of a larger force when focusing is applied. On average, molecules will be further away from the center of the trap when the focusing force is applied than they are while being defocused. Provided that the right switching frequency is chosen, this results in a net focusing of HFS molecules.

III. STABILITY AND ACCEPTANCE

A. Motion in the ac trap

Trapping molecules in an ac trap is a dynamical process that critically depends on the interplay between the applied voltages and switching frequency. The force acting on a polar molecule in an inhomogeneous electric field $\vec{E}(\vec{r})$ of magnitude $E=|\vec{E}|$ is given by

$$\vec{F}(\vec{r}) = -\vec{\nabla} W(E(\vec{r})), \tag{1}$$

with $W(E(\vec{r}))$ denoting the Stark energy. For our experiments we used ammonia (i.e., $^{15}ND_3$) in its $|JK\rangle = |11\rangle$ state as a prototypical polar molecule. The Stark effect of ND_3 is almost linear for electric field strengths in the 5–20 kV/cm region that is relevant in our trap. Below 5 kV/cm, the Stark effect shows a quadratic dependence on the electric field strength. The Stark energy of $^{15}ND_3$ molecules in their $|JK\rangle = |11\rangle$ state is given by

$$W(E) = \pm \sqrt{\left(\frac{W_{\text{inv}}}{2}\right)^2 + \left(\frac{\mu E}{2}\right)^2} \mp \frac{W_{\text{inv}}}{2}, \tag{2}$$

as long as interactions with higher lying $|JK\rangle$ states can be neglected [15]. $W_{\text{inv}} = 1430.336$ MHz is the inversion splitting [16] and $\mu = 1.48$ D the dipole moment [17] of $^{15}ND_3$. At an electric field strength of 10 kV/cm the Stark energy of $^{15}ND_3$ in its $|J, MK\rangle = |1,1\rangle$ HFS energy level amounts to 0.13 cm^{-1}. The slope of the Stark curve in the region of interest is approximately constant and equals -0.013 $cm^{-1}/(kV/cm)$ at the field in the trap center (13 kV/cm for trap voltages of ± 6.6 kV).

For stability analysis of molecular trajectories it is instructive to start with linearized equations of motion. A harmonic ansatz is therefore used to express the Stark energy of a molecule in the field configurations $E_1(x,y,z)$ (focusing 1) and $E_2(x,y,z)$ (focusing 2). For the trap under investigation the resulting equations turn out to be Hill equations for x and y whereas the equation determining the z motion is that of a harmonic oscillator. Due to the symmetry of the applied fields $E_1(x,y,z)$ and $E_2(x,y,z)$ the corresponding Stark energies $W_1(x,y,z)$ and $W_2(x,y,z)$ may be expanded as

$$\begin{aligned} W_1(\vec{r}) &= W(E_1(x,y,z)) \\ &= w_{1,0} + w_{1,x}x^2 + w_{1,y}y^2 + w_{1,z}z^2 \end{aligned} \tag{3}$$

and

$$\begin{aligned} W_2(\vec{r}) &= W(E_2(x,y,z)) \\ &= w_{2,0} + w_{2,x}x^2 + w_{2,y}y^2 + w_{2,z}z^2. \end{aligned} \tag{4}$$

Since the divergence of the force field vanishes at $(x,y,z) = (0,0,0)$ $(\Delta W = 0)$, the expansion coefficients w_{1,r_i} and w_{2,r_i} have to obey

$$w_{i,x} + w_{i,y} + w_{i,z} = 0, \quad i = 1,2. \tag{5}$$

With $W_2(x,y,z) = W_1(-y,x,z)$ it can be further deduced that

$$w_{1,x} = w_{2,y}, \quad w_{1,y} = w_{2,x}, \quad w_{1,z} = w_{2,z}. \tag{6}$$

The time dependence of the Stark energy due to the switching process can be written as

$$W(\vec{r},t) = \frac{W_1(\vec{r}) + W_2(\vec{r})}{2} + \frac{W_2(\vec{r}) - W_1(\vec{r})}{2} f(\omega t). \tag{7}$$

Here, $f(\omega t)$ denotes a square-wave function of angular frequency ω with zero time average

$$f(\omega t) = \begin{cases} 1 & \text{if } W(\vec{r},t) = W_2(\vec{r}), \\ -1 & \text{if } W(\vec{r},t) = W_1(\vec{r}). \end{cases} \tag{8}$$

We further introduce the dimensionless time

$$\tau = \frac{\omega}{2} t \tag{9}$$

and the corresponding second derivative with respect to time

$$\frac{d^2}{dt^2} = \frac{\omega^2}{4} \frac{d^2}{d\tau^2}, \tag{10}$$

so as to define dimensionless parameters

$$a_{r_i} = 4 \frac{(w_{1,r_i} + w_{2,r_i})}{m\omega^2}, \quad r_i = x,y,z \tag{11}$$

and

$$q_{r_i} = 2 \frac{(w_{2,r_i} - w_{1,r_i})}{m\omega^2}, \quad r_i = x,y,z. \tag{12}$$

For these parameters Eqs. (5) and (6) imply

$$a_x = a_y = -a_z/2 \equiv a, \quad a \leq 0 \tag{13}$$

and

$$q_x = -q_y \equiv q, \quad q_z = 0. \tag{14}$$

A parameter value of $a = 0$ would correspond to an infinitely long trap, i.e., a two-dimensional guide where the electric field is constant along z due to symmetry [12,13]. The linear ac trap presented here has finite length. The fringing fields therefore lead to a decrease of field strength along z with increasing distance from the trap center, resulting in a positive a_z and thus $a < 0$.

Now, the equations of motion can be expressed in the following form:

$$\ddot{x} + [a + 2q\ f(2\tau)]x = 0, \tag{15}$$

$$\ddot{y} + [a - 2q\ f(2\tau)]y = 0, \tag{16}$$

$$\ddot{z} - 2az = 0, \tag{17}$$

where the derivation is now with respect to τ. Equations (15) and (16) have the form of a Hill equation which in general reads as

$$\ddot{u} + k(2\tau)u = 0, \tag{18}$$

where $k(2\tau)$ is a periodic function. This equation has two linearly independent solutions $u_1(\tau)$ and $u_2(\tau)$ which can be determined following the so-called Floquet theorem

$$u_1(\tau) = e^{\mu\tau} p(\tau), \tag{19}$$

$$u_2(\tau) = e^{-\mu\tau} p(-\tau), \tag{20}$$

where p is a π-periodic function. The parameter μ is the Floquet exponent and determines the stability of the two solutions. Stable trajectories, i.e., bounded solutions, exist for purely imaginary $\mu \equiv i\beta$. In that case the real valued param-

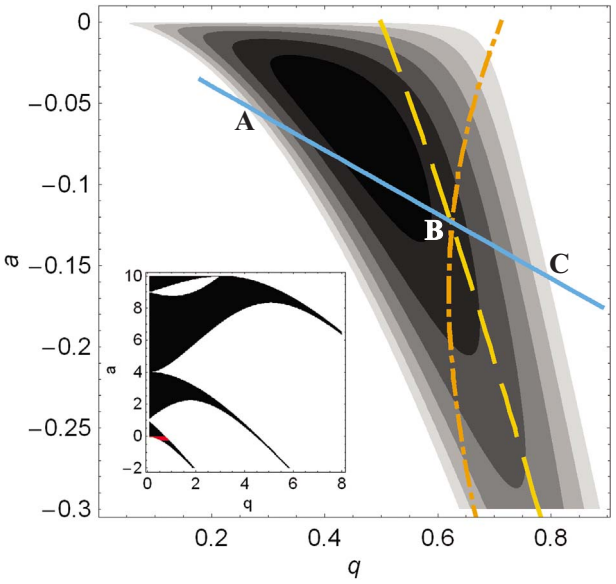

FIG. 2. (Color online) Stability diagram of the linear ac trap as a function of $(q,\ a)$. The inset gives a general overview of the trap's stability diagram while the relevant part for the operation of the trap is enlarged. The different gray colors indicate stable trapping with an increasing trap acceptance for increasing darkness. The solid gray line is the operating line for our linear ac trap using $^{15}ND_3$. The crossings of the operating line with the edges of the stable region are marked by A and C. The dashed straight line (yellow) is the so-called $\beta=\frac{1}{2}$ isobeta line (see text). The dashed-dotted line (orange) corresponds to a resonance caused by coupling between radial and axial motion. The crossing of the operating line with the resonance lines is marked with B.

eter β denotes the fundamental frequency of a particle's motion in the dimensionless time τ. On the other hand, a nonvanishing real part leads to an exponential increase of the amplitude of the particle's trajectory in which case the motion is said to be unstable.

For practical purposes the parameters a and q, as introduced in Eqs. (11) and (12), are better suited to describe the stability. This parameter set is usually employed for the characterization of quadrupole mass filters and Paul traps in ion physics. The parameter a is a measure of the force constant averaged over the switching frequency, whereas the parameter q characterizes the change in the force constant over a switching cycle. Especially for square-wave-like switching of the trapping fields it is straightforward to calculate the stability in terms of these parameters using transfer matrices [18]. The result of such a calculation for a given range of parameters a and q is shown in the inset of Fig. 2. The white areas correspond to instable motion due to parametric resonances, i.e., the molecules are heated and lost from the trap. The black areas denote conditions under which stable molecular trajectories are found.

From a numerical simulation of the electric trapping fields inside the ac trap followed by a polynomial fit to the field data, the operating point as a function of the applied trapping voltage $(+V,-V)$ and the switching frequency ω can be calculated. By assuming $^{15}ND_3$ to have a linear Stark effect for the given electric field, the operating point can be calculated according to

$$(q,a) = \frac{V}{\omega^2}(4.3 \times 10^3, -8.4 \times 10^2), \tag{21}$$

with the voltage V in V and ω in Hz. a and q show the same dependence on V and ω. The quotient a/q is a constant and thus Eq. (21) defines a straight line in the (q,a) plane, i.e., the operating point as a function of the applied high voltages and the switching frequency. This operating line is displayed in Fig. 2. The intersection points of the operating line with the edges of the stability region are labeled A and C.

B. Linear stability and acceptance

Within the harmonic approximation, i.e., as long as anharmonic contributions to the electric fields and nonlinear Stark-effect contributions are neglected, the stability of a particle's trajectory is independent of its starting point in phase space. The operating point (a,q) alone determines whether a trajectory remains finite or not, i.e., whether it is stable or unstable. This dependence is shown in the inset of Fig. 2. White areas indicate regions of unstable motion, while the black areas correspond to regions of stable motion. To arrive at a correct description of a trap's performance the limited extension of the trapping fields has to be considered as well. Therefore, the concept of acceptance is useful. The acceptance of a trap is the set of initial positions in phase space from which a molecule is unable to leave the physical boundaries of the trap. Figure 2 shows a contour plot of the phase-space acceptance of the ac trap in this modified harmonic approximation. The acceptance increases with increasing darkness, i.e., light gray areas correspond to smaller and dark gray areas to larger acceptance. In particular, the white areas are regions of zero acceptance and unstable motion. As mentioned before, the operating point is restricted to negative a values since HFS molecules would otherwise be expelled along z. The magnitude of the acceptance decreases within the stable regions with decreasing a. It also decreases when the operating point approaches the stability boundaries (Fig. 2). When approaching these boundaries in the (a,q) diagram, the molecules are ever more loosely confined and for given initial conditions the maximum distance of a molecule from the trap center increases.

Figure 3 shows typical trajectories of trapped molecules in the x direction with trapping time for three different operating points (a,q) obtained from our numerical simulations using real trapping fields and the real Stark effect without further assumptions. For an operating point (a,q) close to the high frequency end of the stable area (small q, marked as A in Fig. 2) the motion of a molecule can be described as a slow secular motion with a large amplitude, modulated with a high frequency micromotion with a small amplitude. For increasing q, close to B in Fig. 2, the frequency of the slow motion increases, and the fast micro motion becomes more apparent. For the high-q end of the stability diagram, i.e., for low switching frequencies (close to C in Fig. 2), a separation in slow and fast motion is not possible anymore.

C. Nonlinear resonances

The above description of stability in an ac trap employing linearized equations of motion is limited to molecular trajec-

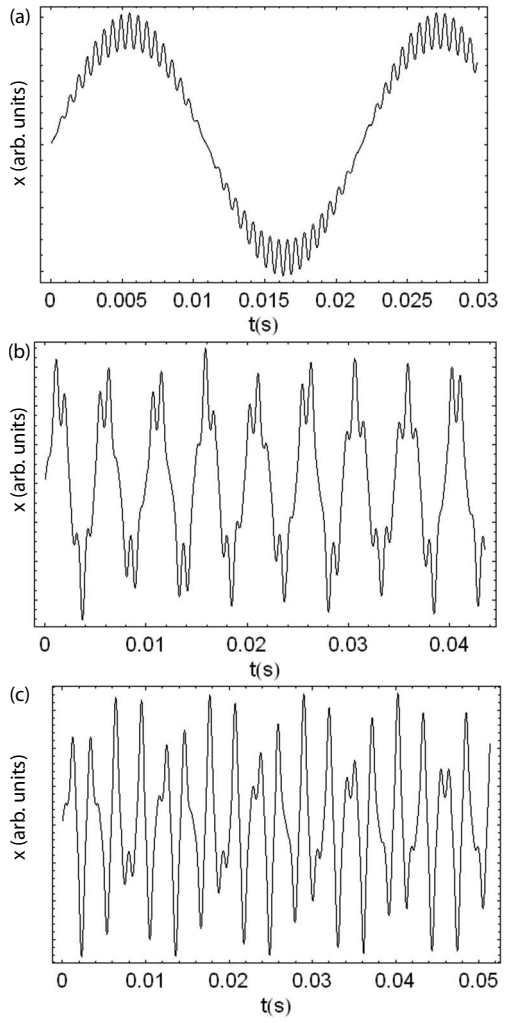

FIG. 3. Typical trajectories of trapped molecules for three different operating points, numerically calculated for the real trapping fields and Stark effects. (a) Close to operating point *A*, (b) close to operating point *B*, and (c) close to operating point *C*.

tories close to the center of the trap since only there the electric field strength is of the desired harmonic form. The further a molecule departs from the trap center the larger becomes the influence of anharmonic field terms that alter the ideal shape. The inclusion of these terms is essential for a correct description of the phase-space dynamics, since it is these contributions that limit the phase-space acceptance of a real ac trap. This reflects the primary difference between trapping ions in quadrupole potentials and ac trapping of molecules: Anharmonic contributions to the electrostatic potential in quadrupole ion traps are only due to nonideal electrodes [19] whereas anharmonicity cannot be avoided in an ac trap for polar molecules. This stems from the different types of interactions of ions and molecules with an electric field. While for ions the interaction energy is proportional to the potential, it depends on the norm of the electric field (or to the norm of higher orders of the electric field) for polar molecules. Since in ac traps the electric field can never be chosen to be harmonic, which actually is possible for the potential, anharmonic contributions cannot be avoided for ac trapping of polar molecules.

The stability of motion in a dynamic trap is based on the fact that the attractive forces on a particle increase with increasing distance from the center. In an ideal harmonic trap this is always true. The main influence of anharmonicity is to reduce and eventually to reverse this effect, at least along certain directions, so that the conditions for stability may not be fulfilled anymore for all particles at the same time. When we consider these anharmonic terms we find that the electric field itself, rather than the physical boundaries of the trap, limits the oscillation amplitude of the particles. The stability therefore does not depend anymore on the operating point alone but also on the starting points in phase space of the loaded particles.

The effects due to the anharmonicity of the fields depend strongly on the exact shape of the potential energy surfaces. Certain analytical methods have been found to approximate these effects quantitatively. However, the application of these methods is in general restricted to the surroundings of certain points in the stability diagram, such as the point $q=a=0$, where the so-called adiabatic potential method may be used [20]. This is often sufficient for the approximate description of the anharmonic motion of ions in dynamic particle traps over a certain range of high frequency forcing. A global analytical description of the phase-space dynamics, however, is not possible anymore, so that numerical simulations of the phase-space dynamics become absolutely necessary. On the other hand, some interesting features can simply be explained by the existence of anharmonic contributions of certain orders with respect to the expansion of the energy surfaces in the coordinates.

Resonances are caused by the degeneracy of motional frequencies. In addition to the parametric resonances that appear through the linear forcing (white regions of instability in the diagram), nonlinear resonance lines, each representing the influence of a certain order of anharmonicity, run through the whole stability diagram. These nonlinear motional resonances occur if the fundamental frequency of a particle's motion is a certain rational multiple of the forcing frequency. The understanding of such nonlinear resonances is crucial, for example, for the safe operation of particle accelerators, in high-resolution ion physics and mass spectrometry. General criteria for the occurrence of these resonances in the motion of dynamically stabilized particles can be derived [21,22]. For a motion in three-dimensional space one obtains

$$n_x\frac{\beta_x}{2}+n_y\frac{\beta_y}{2}+n_z\frac{\beta_z}{2}=n \tag{22}$$

with $|n_x|+|n_y|+|n_z|=N$, n_x, n_y, n_z, $n\in\mathbb{Z}$, and $N\in\mathbb{N}$. N denominates the order of the resonance. $\frac{\beta_x}{2}\omega$, $\frac{\beta_y}{2}\omega$, and $\frac{\beta_z}{2}\omega$ are the fundamental frequencies of the nonperturbed motion in x, y, and z direction, respectively. The main contribution to a given resonance of the order N comes from forces with a nonlinear position dependence of the order $N-1$ for these coordinates [21,22]. In a symmetric ac trap the expansion of the magnitude of the electric field and therefore of the Stark energy of a HFS or LFS molecule in terms of coordinates contains only even orders. The first deviation from the ideal harmonic form appears in fourth order and the lowest order

of an anharmonic resonance is therefore $N=4$.

In the linear ac trap the fundamental frequencies of x and y motion must be equal ($\beta_x=\beta_y=\beta$). Furthermore, the unperturbed fundamental frequency of z motion is just $\sqrt{a_z}=\sqrt{-2a}$ and Eq. (22) simplifies to

$$(n_x+n_y)\frac{\beta}{2}+n_z\frac{\sqrt{-2a}}{2}=n. \tag{23}$$

This equation manifests a relationship between β and a and defines a set of "resonance lines" in the stability diagram. Figure 2 shows two such lines representing resonances of order $N=4$. The dashed line corresponds to a purely radial resonance only involving x and y motion. This line coincides with the isobeta line $\beta=\frac{1}{2}$, i.e., the particles' fundamental frequency of transverse oscillation in a harmonic ac trap would be $\frac{1}{4}$ of the forcing frequency. The dashed-dotted line in contrast represents resonant energy transfer to the axial motion via its coupling to x or y components. Both lines cross the operating line of the trap at the same point. The intersection point of the operating line for our trap with the isobeta line $\beta=\frac{1}{2}$ is labeled "B." The corresponding coordinates are

$$(q,a)=(0.62,-0.12). \tag{24}$$

We studied the influence of the two types of resonances independently using numerical simulations and found that the purely radial resonances involving only x and y motion lead to a significant loss of particles from the trap, whereas the coupling with axial motion is not important.

D. Numerical simulations

The two different electric field configurations of the trap, displayed in Fig. 1, have been simulated using a finite element program (COMSOL, Multiphysics). The magnitude of the electric field and the field gradient vectors were exported on a grid with sampling periods of 0.1 mm and were implemented into the program package LIBCOLDMOL [23], which allows the numerical calculation of the trajectories of the molecules in the trap as a function of time. Using LIBCOLDMOL, we performed Monte Carlo simulations, assuming molecular packets of initially Gaussian (z,v_x,v_y,v_z) or random uniform (x,y) shape (see Ref. [7] for more details). The trajectories of typically one million molecules were calculated by integrating the equations of motion in the Runge-Kutta formalism [Cash-Karp (4,5) or Prince-Dormand (8,9)]. The results of these simulations fit well with the experimental results and are presented along with the experimental data in Sec. V.

IV. EXPERIMENTAL SETUP

In Fig. 4 the experimental setup is shown. In the experiments, the trap is loaded from a Stark-decelerated molecular beam. The details of this part of the experiment are given in Refs. [5,7]. The decelerated packet of $^{15}ND_3$ molecules leaves the decelerator in the low-field seeking (LFS) upper inversion doublet component ($MK=-1$) of the vibronic ground state with a mean velocity of 25 m/s and a velocity spread of ± 7 m/s. The spatial spread of the cold molecular cloud is about ± 1 mm. The exit of the decelerator is about 12.0 mm away from the trap center. The molecules are then further decelerated when entering the trap and brought to a complete standstill in the trap center in the course of the loading process [7]. By applying a resonant microwave pulse of 20 μs duration, which is coupled in using a dipole antenna, about 20% of the molecules are transferred from the LFS upper inversion doublet ($MK=-1$) to the HFS lower inversion doublet ($MK=+1$), i.e., the ground state of para-$^{15}ND_3$. The pumping efficiency is limited by the hyperfine structure of the energy levels of $^{15}ND_3$ [16]. After the microwave pulse is switched off, the ac trap is turned on. The acceptance of the linear ac trap has been experimentally determined to be about 50 mm^3(m/s)^3 for trap voltages of ± 6.6 kV and 1150 Hz switching frequency. The initial spatial distribution in the direction of the molecular beam axis is 0.4 mm and the longitudinal velocity, which is still accepted by the trap, is 2.1 m/s, corresponding to a temperature of 2 mK [7].

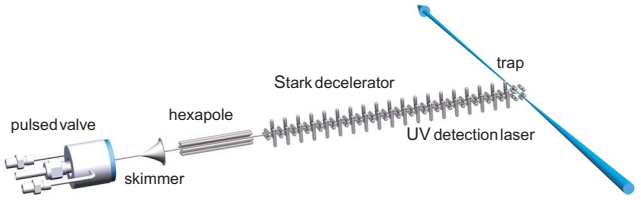

FIG. 4. (Color online) Scheme of the experimental setup of the Stark decelerator-ac trap beamline. The pulsed molecular beam passes a skimmer and is transversally focused by the hexapole onto the entrance region of the decelerator. After deceleration, the molecules are loaded into the trap. The overall length of the beamline is about 1 m.

In the experiments, voltages up to ± 10 kV have been applied to the trap electrodes. After a certain trapping time, the trap is turned off and the molecules are ionized in a state-selective (2+1)-resonance enhanced multiphoton ionization (REMPI) scheme, using a pulsed UV-laser around 321 nm to ionize molecules in the lower component of the inversion doublet (HFS state) and 317 nm to ionize molecules in the LFS higher component of the inversion doublet [24]. The parent ions are detected in a time-of-flight (TOF) mass spectrometer. Using a 75 cm lens the ionization laser is focused into the trap. Because of the very open trap arrangement very good optical access is guaranteed. The laser focus is estimated to be about 200 μm in diameter and the ions can be detected over a length of about 4 mm along the laser beam. Using a computer controlled translation stage, the laser focus can be moved along the molecular beam axis over the whole width of the inside of the trap, enabling the experimental characterization of the spatial distribution of the trapped molecules.

For a detailed study of the stability of the linear ac trap we performed measurements for several experimental conditions, i.e., for several trap voltages and switching frequencies. For different voltages not only the trapping, but also the deceleration and loading fields of the trap are changed. We

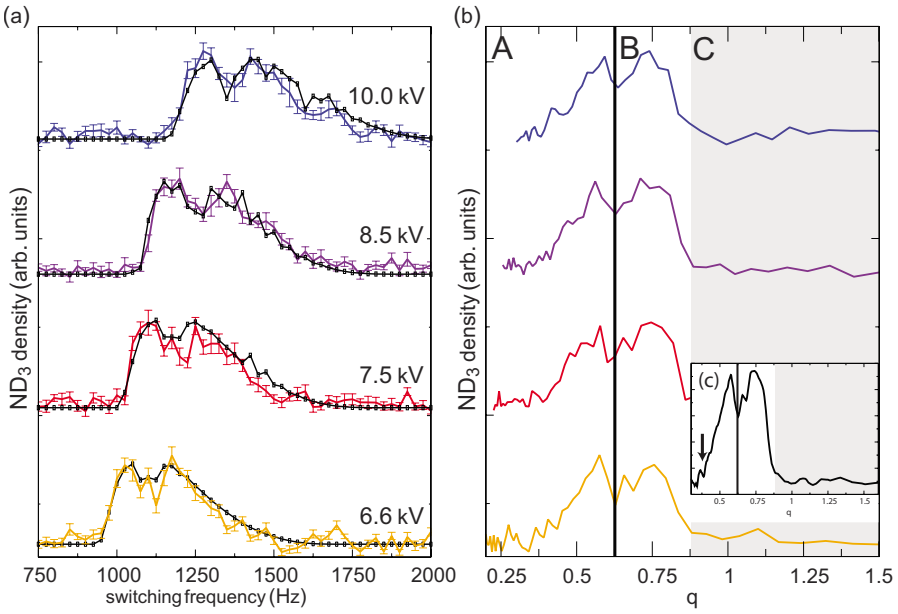

FIG. 5. (Color online) Color online. (a) Frequency dependence of the density of trapped ND_3 for four different trapping voltages, after about 60 ms of trapping time. Both experimental results (with error bars) and simulations (squares) are shown. (b) Dependence of the density of trapped ND_3 on the stability parameter q for the four different trapping voltages. The transition to instable trapping areas (A and C) are marked, as is the nonlinear resonance at B. The gray part marks the area of unstable trapping. (c) Average of the four different curves from (b).

have applied evolutionary strategies to optimize both the loading and the trapping for different sets of trap voltages, i.e., we have adjusted the length of the deceleration and loading steps using the trap, the time when the microwave pulse for pumping the ND_3 from the LFS to the HFS state is applied and the switching frequency, after we had manually determined the optimal conditions for trap voltages of ± 6.6 kV. The optimization of a Stark decelerator beamline using evolutionary strategies has been reported before [25], and we refer to this article for a detailed description of the procedure.

V. EXPERIMENTAL RESULTS AND DISCUSSION

As discussed in detail in Sec. III the applied trap voltages and the switching frequency, i.e., the operating point, largely determine the stability of a dynamic trap for neutral molecules. Furthermore, the acceptance decreases toward the edges of the stable regions (Fig. 2). We determined the density of $^{15}ND_3$ molecules after trapping them for about 60 ms using four different trap voltages (± 6.6 kV, ± 7.5 kV, ± 8.5 kV, and ± 10.0 kV). The applied switching frequency was changed from 700–2000 Hz in steps of 25 Hz. The results are shown in Fig. 5(a) along with the outcome from numerical simulations, which show a very good agreement with the experimental data. As can be seen, the intensity of trapped molecules varies significantly with the switching frequency. With increasing switching frequency a regime of stable trapping is reached, which spans a range of about 400 Hz. Eventually, the signal intensity is slowly decreasing approaching zero for high frequencies. This general behavior is found for all four trap voltages. With increasing trap voltages the optimal trap performance is shifted to higher switching frequencies. Note the clear decrease in signal intensity at around 1100 Hz for ± 6.6 kV, which is also present—shifted to higher frequencies—for the higher trap voltages and which corresponds to molecule losses due to a resonance.

More information can be gained by displaying these data as a function of the stability parameter q, according to Eq. (21) [Fig. 5(b)]. As can be seen, all four curves are now congruent. The stable trapping region is bordered by A for the high-frequency end (low q) and C for the low-frequency end (high q). The observed decrease in signal intensity coincides with the intersection point of the isobeta line for $\beta=\frac{1}{2}$ $(n_x+n_y=4, n_z=0)$ and the nonlinear resonance coupling axial and radial motion $(n_x+n_y=2, n_z=2)$ with the operating line (indicated by B), making an experimental distinction between both types of resonances impossible in our present setup. As mentioned above, numerical simulations indicate that only the purely transverse resonance has a significant influence on the motion of the molecules.

A detailed investigation of the strength of the resonance is beyond the scope of this article. However, it can be concluded that this resonance must indeed be strong, since we can unambiguously observe it after only about 90 switching cycles (for ± 6.6 kV trapping voltage), which is significantly less than in ion trapping. Thus, due to their strengths, resonances in ac traps are of great importance for further applications such as sympathetic cooling.

Figure 5(c) shows the average of the four different curves displayed in Fig. 5(b). In this curve, an additional resonance (indicated by an arrow) might be visible at about $q=0.39$ which would be of sixth order ($N=6$) and purely radial, i.e., only involving x and y motion.

Interestingly, an additional resonance can be found at $q=0.45$ for the measurement with ± 10.0 kV which is not present in the other measurements (Fig. 5). According to our calculations, this resonance is of sixth order ($N=6$) and corresponds to coupling between radial and axial motion $(n_x+n_y=4, n_z=2)$. It appears, therefore, that mixed coupling might be stronger for larger trapping fields.

VI. SUMMARY AND CONCLUSIONS

We have both theoretically and experimentally investigated the stability of a linear ac trap for neutral polar mol-

ecules in high-field seeking states. By adopting the stability theory from ion trapping we have determined the harmonic stability diagram of the linear ac trap. Accounting for the influence of anharmonicity of the trapping fields on the stability, we have indicated possible nonlinear resonances occurring inside the first stability region. Such resonances are inherent for ac traps since anharmonic contributions to the electric field cannot be avoided, in contrast to dynamic ion trapping.

In the experiment, we investigated the trap's performance for various combinations of switching frequencies and trapping voltages. The experiments are accompanied by numerical simulations, showing excellent agreement. The dependence of the measured signal of trapped molecules on both parameters could be explained with the use of the stability diagram. In addition, a clear experimental indication of a nonlinear resonance, namely when the particles' fundamental frequency of transverse oscillation is $\frac{1}{4}$ of the forcing frequency and which was expected from the symmetry of the anharmonicity of the trapping fields, has been observed. The distinct presence of this $\beta=\frac{1}{2}$ resonance after only 90 switching cycles indicates the importance of this strong resonance. A detailed understanding is necessary for future applications using ac traps, such as sympathetic and evaporative cooling to enter the ultracold regime, and for a general, deeper understanding of ac trapping, AG deceleration and ac guiding. From the analysis of our experimental data we can conclude that the stability theory we employed, which also considers coupling between different motional components, is well suited to describe the stability of ac traps for neutral polar molecules.

ACKNOWLEDGMENTS

The research of M.S. was made possible through a Liebig stipend of the "Fonds der Chemischen Industrie." We thank J. Küpper, H. L. Bethlem, B. Sartakov, J. van Veldhoven, and H. Haak for fruitful discussions.

[1] J. Doyle, B. Friedrich, R. V. Krems, and F. Masnou-Seeuws, Eur. Phys. J. D **31**, 149 (2004).
[2] H. L. Bethlem and G. Meijer, Int. Rev. Phys. Chem. **22**, 73 (2003).
[3] H. L. Bethlem, M. R. Tarbutt, J. Küpper, D. Carty, K. Wohlfart, E. A. Hinds, and G. Meijer, J. Phys. B **39**, R263 (2006).
[4] T. Takekoshi, B. M. Patterson, and R. J. Knize, Phys. Rev. Lett. **81**, 5105 (1998).
[5] J. van Veldhoven, H. L. Bethlem, and G. Meijer, Phys. Rev. Lett. **94**, 083001 (2005).
[6] H. L. Bethlem, J. van Veldhoven, M. Schnell, and G. Meijer, Phys. Rev. A **74**, 063403 (2006).
[7] M. Schnell, P. Lützow, J. van Veldhoven, H. L. Bethlem, J. Küpper, B. Friedrich, M. Schleier-Smith, H. Haak, and G. Meijer, J. Phys. Chem. A **111**, 7411 (2007).
[8] H. L. Bethlem, G. Berden, and G. Meijer, Phys. Rev. Lett. **83**, 1558 (1999).
[9] S. Schlunk, A. Marian, P. Geng, A. P. Mosk, G. Meijer, and W. Schöllkopf, Phys. Rev. Lett. **98**, 223002 (2007).
[10] M. R. Tarbutt, H. L. Bethlem, J. J. Hudson, V. L. Ryabov, V. A. Ryzhov, B. E. Sauer, G. Meijer, and E. A. Hinds, Phys. Rev. Lett. **92**, 173002 (2004).
[11] K. Wohlfart, F. Grätz, F. Filsinger, H. Haak, G. Meijer, and J. Küpper, Phys. Rev. A **77**, 031404(R) (2008).
[12] F. Filsinger, U. Erlekam, G. von Helden, J. Küpper, and G. Meijer, Phys. Rev. Lett. **100**, 133003 (2008).
[13] S. A. Rangwala, T. Junglen, T. Rieger, P. W. H. Pinkse, and G. Rempe, Phys. Rev. A **67**, 043406 (2003).
[14] D. Auerbach, E. E. A. Bromberg, and L. Wharton, J. Chem. Phys. **45**, 2160 (1966).
[15] C. H. Townes and A. L. Schawlow, *Microwave Spectroscopy* (Dover, New York, 1975).
[16] J. van Veldhoven, J. Küpper, H. L. Bethlem, B. Sartakov, A. J. van Roij, and G. Meijer, Eur. Phys. J. D **31**, 337 (2004).
[17] R. L. Bhattacharjee, L. H. Johnston, G. R. Sudhakaran, and J. C. Sarker, J. Mol. Spectrosc. **138**, 38 (1989).
[18] N. Konenkov, M. Sudakov, and D. Douglas, J. Am. Soc. Mass Spectrom. **13**, 597 (2002).
[19] R. Alheit, S. Kleineidam, F. Vedel, M. Vedel, and G. Werth, Int. J. Mass Spectrom. **154**, 155 (1996).
[20] D. Gerlich, Adv. Chem. Phys. **82**, 1 (1992).
[21] Y. Wang, J. Franzen, and K. Wanczek, Int. J. Mass Spectrom. **124**, 125 (1993).
[22] A. Drakoudis, M. Sllner, and G. Werth, Int. J. Mass Spectrom. **252**, 61 (2006).
[23] J. Küpper and F. Filsinger, LIBCOLDMOL*: A Particle Trajectory Calculation Framework* (2003–2008), http://libcoldmol.cold-molecules.info
[24] M. N. R. Ashfold, R. N. Dixon, N. Little, R. J. Stickland, and C. M. Western, J. Chem. Phys. **89**, 1754 (1988).
[25] J. J. Gilijamse, J. Küpper, S. Hoekstra, N. Vanhaecke, S. Y. T. van de Meerakker, and G. Meijer, Phys. Rev. A **73**, 063410 (2006).